Cellular and Molecular Life Sciences (2025) 82:206
https://doi.org/10.1007/s00018-025-05709-6

ORIGINAL ARTICLE

Aberrant downregulation of Y-box binding protein 1 expression impairs the cell cycle in an m^{5}C-dependent manner in human granulosa cells from patients with primary ovarian insufficiency

Qichao Chen[1,2] · Sisi Wang[1,2] · Min Zhang[1,2] · Yu Xiang[1,2] · Qingqing Chen[1,2] · Zhekun Li[1,2] · Yang Song[1,2] · Long Bai[1,2,3] · Yimin Zhu[1,2,3,4]

Received: 16 July 2024 / Revised: 1 April 2025 / Accepted: 9 April 2025

Abstract

Y-box binding protein 1 (YBX1) has been reported to play a role in human granulosa cell (GC) dysfunction by binding with long noncoding RNAs in patients with primary ovarian insufficiency (POI). 5-Methylcytosine (m^{5}C) methylation is an abundant RNA epigenetic modification that is widely present in eukaryotic RNAs. However, whether YBX1, an important m^{5}C reader, whether YBX1 participates in POI in an m^{5}C- dependent manner remains unknown. Here, we demonstrated that the expression levels of YBX1 were decreased in GCs from patients with biochemical POI. YBX1 knockdown in a human granulosa cell line (KGN) impaired cell proliferation by preventing the G1 to S transition in the cell cycle. Conversely, YBX1 overexpression promoted the KGN cell proliferation. Integrated analysis of the transcriptome and m^{5}C methylome profiles revealed that in human GCs, knockdown of YBX1 expression destabilized cell cycle-associated transcripts in an m^{5}C-dependent manner, resulting in cell cycle arrest. Our results provide new insights of the pathogenesis of POI, revealing an alternative molecular mechanism in which YBX1 participates in human GC dysfunction by affecting the stability of cell cycle-associated genes in an m^{5}C-dependent manner and thereby modulating GC proliferation.

Keywords YBX1 · M5C · Cell cycle · Granulosa cell · Primary ovarian insufficiency

Introduction

Primary ovarian insufficiency (POI) is a severe reproductive disease in women of childbearing age, with an estimated prevalence of 2–4% in the population [1]. Clinically, POI is defined as cessation of menstruation prior to the age of 40 years and is characterized by elevated serum follicle-stimulating hormone (FSH > 25 IU/L), lower serum estradiol and symptoms associated with estrogen deficiency [2]. POI development can be divided into three phases according to its pathological characteristics: the occult, biochemical and overt stages. At the biochemical stage, POI is distinguished by elevated serum FSH levels and reduced fertility but regular menses [2]. To date, several etiological factors of POI have been identified, including genetic predisposition, autoimmune-mediated ovarian damage, infectious agents, and iatrogenic interventions. However, it remains difficult for clinicians to prevent and treat the occurrence of POI due to its high degree of heterogeneity.

In recent years, many questions regarding RNA modifications has been resolved wtih the rapid innovations in

Qichao Chen, Sisi Wang and Min Zhang contributed equally.

Long Bai and Yimin Zhu jointly supervised this work.

✉ Long Bai
bailong0375@zju.edu.cn

✉ Yimin Zhu
zhuyim@zju.edu.cn

1 Key Laboratory of Reproductive Genetics (Ministry of Education), Women's Hospital, Zhejiang University School of Medicine, Hangzhou 310002, Zhejiang, China

2 Department of Reproductive Endocrinology, School of Medicine, Women's Hospital, Zhejiang University, Hangzhou 310002, Zhejiang, China

3 Zhejiang Key Laboratory of Maternal and Infant Health, Women's Hospital, Zhejiang University School of Medicine, Hangzhou 310002, Zhejiang, China

4 Institute of Medical Genetics and Development, Zhejiang University, Hangzhou 310002, Zhejiang, China

Published online: 21 May 2025

detection methodologies [3]. More than 170 post-transcriptional RNA modifications have been identified [4]. These diverse modifications regulate mRNA fate by promoting stability, splicing, nuclear export, or turnover [5]. In the female reproductive system, the essential roles of RNA modifications, mainly N^6-methyladenosine (m^6A) modifications, in ovarian development, oocyte maturation, and embryo development have been well documented in animal studies [6]. Furthermore, aberrant RNA modifications have been reported to be involved in female reproductive diseases including POI, polycystic ovary syndrome (PCOS), and endometriosis [7]. 5-Methylcytosine (m^5C) is another known epigenetic modification that is abundant in both mRNAs and noncoding RNAs [8–10]. To date, studies on m^5C modifications in the female reproductive system have focused on exploring the functional roles of m^5C in oocyte maturation and embryogenesis events [11–15]. However, little is known about the role of m^5C in female reproductive diseases. TRDMT1, a highly conserved RNA methyltransferase, has been reported to participate in DNA damage repair in granulosa cells (GCs) in POI patients by mediating RNA m^5C methylation, highlighting the involvement of RNA m^5C modification in POI [16].

Consistent with m^6A modifications, a trio of proteins known as writers, readers, and erasers, collectively regulate the dynamic changes in m^5C modifications [17]. Writers are responsible for depositing m^5C marks on the target mRNA, erasers remove the m^5C modification from the RNA, and readers recognize m^5C-containing RNAs and determine their fates [15, 18, 19]. Y-box binding protein 1 (YBX1) is a known m^5C reader. YBX1 was first identified as a nucleic acid binding-protein that regulates the transcription of follicle-stimulating hormone (FSH)-responsive genes [20]. It has been reported that YBX1 participates in GC dysfunction in POI by regulating MSH5 expression [21]. A recent study demonstrated that exosomal YBX1 facilitates ovarian restoration by the MALAT1/miR-211-5p/FOXO3 axis [22]. However, as a well-known m^5C reader protein, whether YBX1 plays a pathogenic role in POI patients in an m^5C-dependent manner remains elusive.

To address these questions, we investigated the role and underlying mechanism of YBX1-mediated m^5C modification alternations in the pathogenesis of POI. Our results demonstrated that the transcriptional and protein expression levels of YBX1 were decreased in GCs from POI patients. Silencing endogenous *YBX1* expression impaired the cell proliferative ability of KGN, an immortalized human granulosa cell model. Conversely, overexpressing *YBX1* in KGN cells promoted cell proliferation. Mechanistically, we demonstrated that YBX1 governed the stability of G1-S phase-related mRNAs in an m^5C-dependent manner.

Materials and methods

Ethical statement and patients

This study was approved by the Ethics Committee of Women's Hospital of Zhejiang University (File No. IRB-20230043-R). All participants provided signed informed consent. Each participant was recruited from the cohort of patients undergoing in vitro fertilization (IVF) at the Women's Hospital, School of Medicine, Zhejiang University between March 2021 and December 2024. The trial enrolled 87 participants in total, including 40 patients diagnosed with bPOI and 47 control subjects. The clinical characteristics of the controls and the bPOI patients are summarized in Table 1. The inclusion criteria for patients followed the diagnostic criteria for bPOI: (i) basal serum FSH ≥ 10 IU/L; (ii) age < 40 years; (iii) menstrual cycle duration between 23 and 35 days; and (iv) ovarian antral follicle count (AFC) < 10. The control group consisted of infertile women undergoing assisted reproductive treatment due to tubal and/or male factors. Exclusion factors included comorbidities such as known chromosomal abnormalities, endometriosis, adenomyosis, autoimmune diseases, prior ovarian surgery, or significant systemic diseases.

Blood samples were obtained from all participants via venipuncture. Following serum separation, concentrations of anti-Müllerian hormone (AMH), follicle-stimulating hormone (FSH), luteinizing hormone (LH), and estradiol were quantified. Antral follicle count (AFC) was assessed by a certified ultrasonographer using transvaginal gynecological ultrasound.

Preparation of human granulosa cells

On the day of oocyte retrieval, follicular fluid was collected from each participant. The sample was centrifuged at 3000 rpm for 10 min and the supernatant was discarded. Then, the pellet was resuspended in saline solution, and transferred to lymphocyte separation medium (LTS1077, BD Science, USA). Density gradient centrifugation was performed at

Table 1 Clinical characteristics of patients with bPOI and controls

Characteristics	Control (n = 47)	bPOI (n = 40)	*P* value
Age(y)	32.64 ± 3.05	33.80 ± 3.06	0.080
BMI(kg/m^2)	21.36 ± 2.26	21.29 ± 2.70	0.851
Basal FSH (mIU/mL)	6.53 ± 1.51	12.68 ± 3.34	8.0E−15
Basal LH (mIU/mL)	5.09 ± 2.18	5.07 ± 2.18	0.978
Basal estradiol (pg/mL)	127.60 ± 62.39	142.74 ± 88.48	0.368
AMH(ng/mL)	2.92 ± 1.16	0.95 ± 0.47	1.1E−15

2000 rpm for 20 min, and the granulosa cells (GCs) were separated in the intermediate layer. Following a saline solution wash, the GCs were stored at −80 °C until further use.

Immunohistochemical (IHC) staining

Ovaries from 3-week-old wild-type female mice were fixed overnight in 4% paraformaldehyde. The samples were subsequently embedded in paraffin, and 5-μm-thick sections were prepared. Following incubation with the YBX1 (20339-1-AP, Proteintech, China, 1:100)-specific or IgG primary antibody and the corresponding secondary antibody, the sections were stained with hematoxylin and mounted in neutral balsam for observation.

Cell culture

KGN cells [23], a human ovarian cancer granulosa cell line obtained from RIKEN (RRID: CVCL_0375), were cultured in high-Glucose DMEM (C3113-0500, VivaCell Biosciences, China) supplemented with 5% fetal bovine serum (SE100-011, VISTECH, New Zealand) and 1% penicillin–streptomycin (15140-122, Gibco, USA) at 37 ℃ with 5% CO_2.

Cell transfection

KGN cells were transfected with 25 nM siRNA targeting YBX1 (sc-38634, Santa Cruz, USA) to knockdown endogenous YBX1 expression or negative control (sc-37007, Santa Cruz, USA) via Lipofectamine RNAiMAX (13,778,075, Invitrogen, USA) in Opti-MEM (31,985,070, Gibco, USA) when the density of KGN cells reached 70–80%. To overexpress YBX1, KGN cells were transfected with pCMV3-YBX1-HA (HG17046-CY, Sino Biological, China) via Lipofectamine 3000 (L3000015, Invitrogen, USA) in Opti-MEM when the density of KGN cells reached 70–80%. The KGN cells were harvest for further analysis at 48 h after transfection.

RNA extraction and quantitative real-time PCR

Total RNA was extract using RNAiso Plus kit (9109, Takara, Japan) in accordance with the manufacturer's instructions and subsequently reverse transcribed to cDNA using the PrimeScript RT reagent kit (RR037 A, Takara, Japan). The reaction mixture for quantitative real-time PCR had a total volume of 15 μL, consisting of 7.5 μL of ChamQ Universal SYBR qPCR Master Mix (Q711-02, Vazyme, China), 0.6 μL each of forward and reverse primer (10 pmol/μL), 4 μL of cDNA and 2.3 μL of RNase-free water. The experiments were carried out by the Quant Studio™ 5 System (Applied Biosystems, USA) in a 96-well 0.2-mL block. The $2^{-\Delta\Delta Ct}$ formula was used to calculate the relative level of mRNA, with β-actin serving as the reference gene. Supplementary Table 1 shows a list of the primers used for qRT-PCR.

Western blot

After being washed twice with cold PBS, the cells were collected and lysed on ice for 5 min in lysis buffer (#9803, Cell Signaling Technology, USA) containing protease inhibitor cocktail (#5871, Cell Signaling Technology, USA). The protein supernatant was then extracted from the lysates by centrifugation at 12,000 rpm for 10 min. A total of 20 μg of protein was mixed with loading buffer, denatured at 95 ℃ for 5 min, and loaded onto an SDS-PAGE gel. After the protein marker migrated into the separating gel following the initial run of the concentration gel at 90 V, the voltage was increased to 130 V for further separation. The proteins were transferred from the SDS-PAGE gel to PVDF membrane (Bio-Rad, USA), and the membrane was blocked for 1 h with 5% skim milk. The primary antibody was diluted in 5% skim milk and incubated with the membrane at 4 ℃ overnight. The primary antibodies used were as follows: anti-YBX1 (20339-1-AP, Proteintech, China, 1:1000), anti-cyclinD1 (#55506, Cell Signaling Technology, USA, 1:1000), anti-CDK6 (13331, Cell Signaling Technology, USA, 1:1000), anti-CDK4 (#12790, Cell Signaling Technology, USA, 1:1000), and anti-α-Tubulin (66031-1-Ig, Proteintech, China, 1:20000). On the following day, the membrane was washed with 0.1% TBST for 1 h and was incubated with secondary antibody diluted in 5% skim milk at room temperature for 1 h. Afterward, the membrane was washed with TBST for 1 h again. Finally, the immunoreactive protein bands were identified with an enhanced chemiluminescence (ECL) substrate (1705060, Bio-Rad, USA) in the dark.

Cell proliferation assay

Cell proliferation ability was determined with a Cell Counting Kit-8 (BS350B, Biosharp, China) and a Cell-Light™ EdU Apollo in Vitro Kit (C10310-1, Ribo, China). For the CCK-8 assay, KGN cells were transfected with si*YBX1* or siControl for 48 h each and then plated at a density of 2000 cells per well in 96-well plates. This time point was designated 0 h. Then, at 12, 24, 48, and 72 h, 10 μL of CCK-8 solution and 90 μL of DMEM were added to each well, and incubated at 37 ℃ and 5% CO_2 for 2 h. The absorbance at 450 nm was recorded.

For the EdU incorporation assay, KGN cells were transfected with the indicated siRNAs. After 48 h of transfection, KGN cells were plated into 12-well plates. After cell adhesion, the KGN cells were incubated with 50 μM EdU at 37 ℃ and 5% CO_2 for 2 h, in accordance with the manufacturer's protocol. After being washed twice with PBS and fixed with

4% paraformaldehyde at room temperature for 30 min, the KGN cells were treated with 2 mg/ml glycine solution on a shaker for 5 min. Then the cells were permeabilized by adding 0.5% Triton X-100 for 10 min. Following a second round of washing with PBS, the cells were incubated with 1 × Apollo staining reaction solution and Hoechst 33,342 at room temperature on a shaker for 30 min in a light-protected environment. Finally, the cells were washed three times with PBS to remove any residual staining solution. The EdU and nuclear signals were visualized via fluorescence microscopy (Olympus, Japan).

Cell cycle assay

The cell cycle distribution was determined with a Cell Cycle Staining Kit (CCS012, Multi Science, China). A total of 1×10^6 cells were collected and washed with PBS. The cells were incubated with 1 mL of DNA staining solution and 10 µL of permeabilization solution for 30 min at room temperature in the dark followed by flow cytometry (CytoFLEX S, Beckman, USA). The numbers of cells in the G1, S, and G2 phases was determined with FlowJo software (BD Biosciences, USA) to the respective fractions were calculated.

RNA immunoprecipitation (RIP) assay

The RIP assay was carried out as previously described [24]. Briefly, KGN cells at ~ 80–90% of confluence were harvested from 100 mm culture plates. The cells were washed twice with ice-cold PBS and lysed in 250 µL polysome lysis buffer (100 mM KCl, 5 mM $MgCl_2$, 10 mM HEPES–NaOH pH 7, 0.5% Nonidet P-40, 1 mM DTT, 200 units/mL RNase OUT, and EDTA-free protease inhibitor cocktail) for 5 min on ice. Protein A agarose beads (NRPB01L-20, Nuptec, China) were incubated with an anti-YBX1 antibody or an IgG antibody (#2729S, Cell Signaling Technology, USA) at 4 ℃ for 2 h and then 100 µL of whole-cell supernatant was added to the bead mixture and incubated overnight at 4 ℃ with rotation. The beads were washed in quintuplicate with NT-2 buffer (50 mM Tris–HCl pH 7.4, 150 mM NaCl, 1 mM $MgCl_2$, 0.05% NP-40), and RNAiso Plus was added to extract the RNAs that had been bound to the beads; the coprecipitated RNAs were then subjected to qRT-PCR analysis.

Methylated RNA immunoprecipitation (MeRIP) assay

For the MeRIP assay, KGN cells were cultured to 80–90% confluence in 100 mm culture plates, washed twice with cold PBS and then treated with RNAiso Plus for RNA extraction. The extracted RNA was added to Protein A agarose beads conjugated with m^5C antibody (AB214727, Abcam, USA) and incubated at 4 ℃ for 4 h with rotation. After washing five times with IP buffer (0.05 M Tris–HCl, 0.75 M NaCl, 0.5% NP-40, and 200 units/mL RNase OUT), the coprecipitated RNAs were extracted via RNAiso Plus and subjected to qRT-PCR analysis.

RNA stability assay

KGN cells were treated with 5 µg/mL actinomycin D (50–76-0, Med Chem Express, USA) and collected at 0, 2, 4, and 8 h. Total RNA was extracted and qRT-PCR was used to detect the relative expression levels of RNA.

Luciferase reporter assay

The 5'UTR of *CCND1* was cloned and inserted into pGL3-promoter vector (Promega, USA). For the mutant reporter plasmids, cytosine (C) within the m^5C motif, was substituted with thymine (T) or adenosine (A) [25, 26]. HEK293 T cells were seeded into a 6-well plate and cotransfected with 0.5 µg of vector control, *CCND1* 5'UTR WT or mutant reporter plasmids, 0.5 µg of YBX1 overexpression plasmids, and 0.2 µg of pRL-TK plasmids (Renilla luciferase reporter vector) via Lipofectamine-3000 transfection reagent. After 48 h, HEK293 T cells were harvested and luciferase activity was measured by the Dual Luciferase Reporter Gene Assay Kit (11402ES60, Yeasen Biotechnology, China), with normalization to pRL-TK.

RNA-seq and MeRIP-seq

For RNA-seq, total RNA was isolated from YBX1 knockdown and control KGN cells and the rRNAs were removed with a GenSeq® rRNA Removal Kit (GenSeq, China). After rRNA depletion, the samples were subsequently used for library construction following the protocol provided by the GenSeq® Low Input RNA Library Prep Kit (GenSeq, China). The generated sequencing libraries were then subjected to quality control and quantification on the BioAnalyzer 2100 system (Agilent Technologies, USA), followed by 150 bp paired-end sequencing on the Illumina NovaSeq 6000 platform.

The provider of the m^5C-MeRIP-seq service was CloudSeq Inc. (Shanghai, China). In summary, RNA samples extracted from KGN cells that had undergone YBX1 knockdown or control treatment with TRIzol reagent were randomly fragmented into ~ 200 nt fragments. The m^5C antibody was coupled to Protein A/G beads by spinning them at room temperature for 1 h. The fragmented RNA was subsequently incubated with the antibody-bound beads and rotated at 4 °C for 4 h. After multiple washes to eliminate unbound components, the captured RNA was eluted from the complexes and purified. Both the IP and input samples

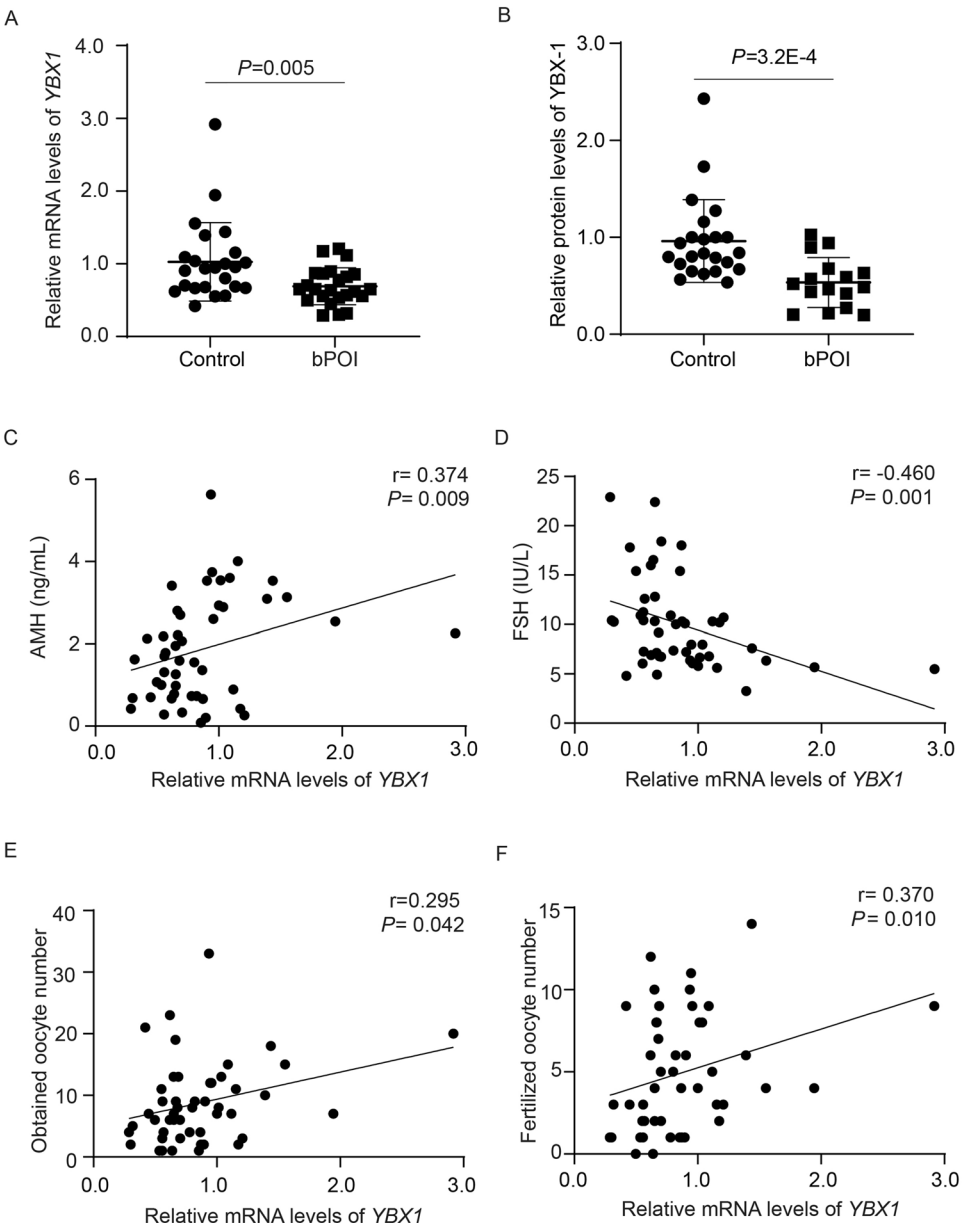

Fig. 1 YBX1 expression levels are decreased in human granulosa cells from bPOI patients. **A** The mRNA expression levels of *YBX1* were determined by qRT-PCR in GCs from an independent cohort of controls (n = 24) and bPOI (n = 24). Data are presented as mean ± SD. **B** The protein expression levels of YBX1 were determined by western blot in GCs from an independent cohort of controls (n = 23) and bPOI (n = 16). Data are presented as mean ± SD. **C**, **D** The correlation analysis of the expression levels of YBX1 in GCs with the serum AMH (**C**) and FSH (**D**) levels. **E**–**F** The correlation analysis of the expression level of YBX1 in GCs with the oocyte retrieval and fertilization outcome indicators, including obtained oocyte number (**E**) and fertilized oocyte number (**F**). *P* value, two-tailed Student's *t* test. n defines replicate samples

were then processed with the GenSeq® Low Input Whole RNA Library Prep Kit (GenSeq, China) for library preparation. Following quality control assessment with an Agilent 2100 Bioanalyzer (Agilent), the constructed libraries were then subjected to high-throughput sequencing on the NovaSeq platform (Illumina).

Sequencing data analysis

Raw RNA-seq data were obtained after sequencing on the Illumina NovaSeq 6000 sequencer, and underwent initial quality control by Q30. Subsequently, Cutadapt software (v1.9.3) was employed for 3' adaptor trimming and to remove low-quality reads, and the retained high-quality clean reads were then aligned to the human reference genome version 19 (hg19) with HISAT2 software (v2.0.4) [27, 28]. After the raw counts were obtained by HTSeq software (v0.9.1), the differentially expressed transcripts were identified, followed by normalization and calculation of the fold change and adjusted *p* values via the edgeR software (v4), with adjusted *p* value ≤ 0.05 and absolute fold change ≥ 2 as criteria [29, 30]. A heatmap was generated with the R package pheatmap. Gene set enrichment analysis was performed with the R package clusterProfiler [31].

For MeRIP-seq, paired end reads were obtained by sequencing on the Illumina NovaSeq 6000 sequencer and subjected to quality control according to the Q30 value. The

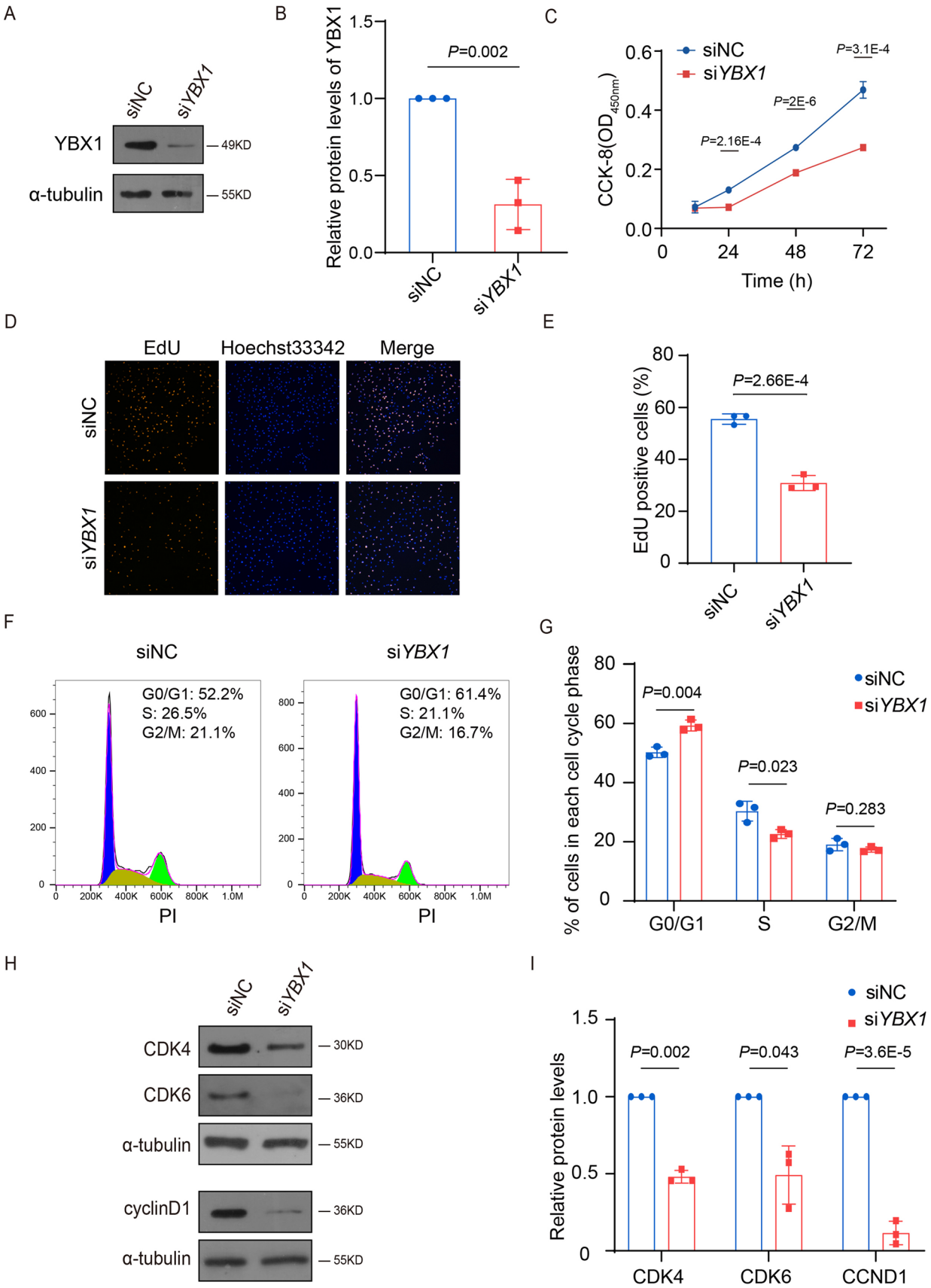
A
siNC
siYBX1
YBX1
49KD
α-tubulin
55KD
B
Relative protein levels of YBX1
P=0.002
siNC
siYBX1
C
CCK-8(OD450nm)
siNC
siYBX1
P=3.1E-4
P=2E-6
P=2.16E-4
Time (h)
D
EdU
Hoechst33342
Merge
siNC
siYBX1
E
EdU positive cells (%)
P=2.66E-4
siNC
siYBX1
F
siNC
siYBX1
G0/G1: 52.2%
S: 26.5%
G2/M: 21.1%
G0/G1: 61.4%
S: 21.1%
G2/M: 16.7%
PI
PI
G
% of cells in each cell cycle phase
siNC
siYBX1
P=0.004
P=0.023
P=0.283
G0/G1
S
G2/M
H
siNC
siYBX1
CDK4
CDK6
α-tubulin
cyclinD1
α-tubulin
30KD
36KD
55KD
36KD
55KD
I
Relative protein levels
siNC
siYBX1
P=0.002
P=0.043
P=3.6E-5
CDK4
CDK6
CCND1

◂**Fig. 2** YBX1 knockdown inhibits cell cycle progression in human granulosa cells. **A**, **B** Level of YBX1 in KGN cells after siRNA silencing was detected by western blot. Data are presented as mean ± SD (n = 3). C. Effects of *YBX1* knockdown on KGN cells proliferation were measured using the CCK-8 assay. Data are presented as mean ± SD (n = 3). **D** The EdU staining revealed the proliferative ability of KGN cells after *YBX1* knockdown. Cells were detected using Hochest staining (blue), while the proliferating cells were identified through EdU staining (red). **E** The percentage of EdU-positive cells in the staining was determined. Data are presented as mean ± SD (n = 3). **F**, **G** The cell cycle distribution of KGN cells after *YBX1* knockdown was assessed using flow cytometry. Data are presented as mean ± SD (n = 3). **H** The expression of G1-S phase-related proteins, including CDK4, CDK6, and cyclin D1 were determined using western blot in KGN cells. **I** The quantification of protein levels normalized to α-tubulin protein expression were presented by graph. Data are presented as mean ± SD (n = 3). *P* value, two-tailed Student's *t* test. n defines technical replicates. *NC* negative control

3' adaptor and low-quality reads were removed using Cutadapt software (v1.9.3) after which the retained high-quality, clean reads of all the libraries were aligned to the human reference genome (hg19) via HISAT2 software (v2.0.4) [27, 28]. The m^5C peaks were called via MACS software and the differentially methylated sites were identified by diffReps (|log2 FC|≥ 1, p value < 0.00001) [32, 33]. Integrative Genomics Viewer was used to visualized the m^5C peaks [31]. Motif enrichment was accomplished with DREME 5.3.0 [34]. Gene Ontology (GO) and Kyoto Encyclopedia of Genes and Genomes (KEGG) enrichment analyses were performed with the DAIVD website, and a false discovery rate (FDR) < 0.05 was considered to indicate statistical significance [35].

Statistics and reproducibility

All experiments were conducted with at least three biological replicates to demonstrate robust reproducibility. Data visualization (graph generation) and analysis were performed via GraphPad Prism 8.0. All the data were presented as the means ± SD. Two-tailed Student's *t* tests were used to compare p values between two groups. The Kolmogorov–Smirnov test was performed to evaluate the normally distribution of sample values before applying the Student's *t* test Correlations were assessed via Spearman correlation analysis. $P < 0.05$ was considered statistically significant.

Results

YBX1 expression levels are decreased in human granulosa cells from bPOI patients

To explore the location of YBX1 expression in the ovary, we performed IHC staining on ovaries from 3-week-old mice. Our results revealed that the YBX1 protein was ubiquitously expressed in various types of ovarian cells (Figure S1). To elucidate the changes in the YBX1 expression in bPOI, we determined the changes in the Y*BX1* transcript and protein levels in hGL cells from bPOI patients and controls who were undergoing IVF procedure. The results revealed that both the mRNA and protein expression levels of YBX1 were significantly lower in hGL cells from bPOI patients than in those from controls (Fig. 1A and B). Pearson correlation analysis revealed that *YBX1* mRNA expression levels in hGL cells were positively correlated with serum AMH levels (Fig. 1C) but negatively correlated with FSH levels (Fig. 1D). Moreover, the *YBX1* mRNA expression levels in hGL cells were positively correlated with IVF outcomes, including the number of obtained oocytes and the number of fertilized oocytes (Fig. 1E and F). These results indicate that YBX1 may participate in POI.

YBX1 regulates cell cycle progression in human granulosa cells

To decipher the role of YBX1 in regulating GC function, endogenous *YBX1* expression in KGN cells was silenced via siRNA, and cell viability was evaluated via CCK-8 assay. The knockdown (KD) efficiency was shown in Fig. 2A and B. The CCK-8 assay revealed that the proliferative ability of KGN cells was significantly decreased after *YBX1* knockdown (Fig. 2C). Moreover, the EdU staining assay revealed that the proportion of EdU-positive cells was dramatically lower in the YBX1-KD cells than the control cells, further confirming that decreasing *YBX1* expression inhibited cell proliferation (Fig. 2D and E). To elucidate the underlying mechanism by which YBX1 regulates of cell proliferation, we examined the cell cycle progression of KGN cells when *YBX1* expression was inhibited. Flow cytometry assay revealed that the percentage of cells in G0/G1 phase was increased after *YBX1* knockdown, whereas the percentage of cells in S phase decreased (Fig. 2F and G). Western blotting results further demonstrated that the inhibition of *YBX1* expression significantly reduced the expression levels of cell cycle regulatory proteins (CDK4, CDK6, and Cyclin D1) (Fig. 2H and I).

To further validate the regulatory role of YBX1 in KGN cell proliferation, we overexpressed YBX1 by transfecting pCMV3-YBX1-HA plasmids into KGN cells. The results demonstrated that YBX1-overexpressing cells exhibited increased proliferative ability (Fig. 3A–F). Moreover, the expression levels of cell cycle regulatory proteins were also increased in the YBX1-overexpressing cells (Fig. 3F and G).

Inhibition of YBX1 expression alters the transcriptome in KGN cells

To gain insight into the mechanism of YBX1-mediated cell cycle progression arrest, the changes in the transcriptome of YBX1-silenced KGN cells were examined via RNA-sequencing (RNA-seq). Heatmap analysis revealed that the transcriptome was altered in YBX1-KD KGN cells (Fig. 4A). In total, 580 upregulated transcripts and 695 downregulated transcripts were detected in YBX1-KD cells (Fig. 4B). Gene Ontology (GO) analysis revealed that the upregulated transcripts were enriched mainly in pathways associated with cell adhesion, extracellular matrix organization, and chemical synaptic transmission (Fig. 4C), whereas the downregulated transcripts were enriched primarily in pathways involved in DNA replication, cell division, the cell cycle, and cell proliferation (Fig. 4D). Gene set enrichment analysis (GSEA) revealed that the downregulated transcripts were significantly enriched in pathways related to the cell cycle and DNA replication (Fig. 4E and F). To further validate our RNA-seq data, several differentially expressed transcripts were selected for examination by RT-qPCR analysis. As shown in Fig. 4G, *CDC25 A, CCND1, E2 F1, CCNE1, MCM4*, and *RCC1* mRNA expression levels were significantly decreased in YBX1-KD KGN cells, consistent with our RNA-seq results.

YBX1 knockdown remodels the m^{5}C methylome in KGN cells

YBX1 has been identified as an m^{5}C reader that regulate gene expression through its recognition of m^{5}C-modified RNAs [36]. Accordingly, we investigated the changes in the m^{5}C methylome landscape in *YBX1*-silenced KGN cells via m^{5}C-MeRIP-seq. The identified m^{5}C peaks were located primarily in exons and were highly enriched near the transcription start site (TSS) and coding sequence (CDS) regions in both the control and *YBX1* KD cells (Fig. 5A and 5B). The binding motif "SSWGGA" was the most enriched motif in both the control and YBX1-KD groups (Fig. 5C). In total, 8428 m^{5}C peaks were significantly altered in YBX1-KD cells, including 5832 hypermethylated peaks in 4432 transcripts and 2596 hypomethylated peaks in 1932 transcripts (Fig. 5D and Supplementary Table 2).

To investigate whether altered m^{5}C methylation affects target transcript expression, a quadrant diagram analysis was performed. The results revealed that 588 and 401 m^{5}C peaks were hypermethylated and hypomethylated, respectively (Fig. 5E). Considering that the YBX1 is an m^{5}C reader, *YBX1* knockdown could decrease m^{5}C methylation levels. Therefore, the subgroup of transcripts with downregulated mRNA expression and m^{5}C methylation levels were of interest. We identified 385 hypomethylated m^{5}C sites in 211 downregulated transcripts in YBX1-KD KGN cells (Fig. 5E). The GO analysis revealed enriched pathways related primarily to DNA replication, the cell cycle and the G1/S transition of the mitotic cell cycle (Fig. 5F).

Identification of YBX1 binding targets involved in the mitotic G1/S transition

To confirm whether the downregulated transcripts with hypomethylated m^{5}C levels were the binding targets of YBX1, our RNA-seq results overlapped with published YBX1-RIP-seq results (GSE159153) in 293 T cells. The Venn analysis results revealed that 111 transcripts overlapped with 211 downregulated transcripts with hypomethylated m^{5}C levels and 7666 YBX1 binding targets (Fig. 6A and B). The cellular functions of this 211 transcript subgroup were enriched in the DNA replication and the cell cycle pathways and in the G1/S transition of the mitotic cell cycle (Fig. 6C).

The m^{5}C modification sites of several target genes involved in the G1/S transition of the mitotic cell cycle, including *CCND1*, *CCNE1* and *RCC1*, were confirmed by IGV analysis (Fig. 6D–F). We observed decreased m^{5}C modification peak levels among these genes in YBX1-KD KGN cells (Fig. 6D–F). Importantly, we found that these m^{5}C modification sites were predominantly located at the TSS and CDS regions, coinciding with reported YBX1 binding sites. The YBX1-RIP-qPCR results further confirmed the ability of YBX1 to bind these transcripts (Fig. 6G). We also investigated the mRNA expression levels *CCND1*, *CCNE1*, and *RCC1* in hGL cells and found that they were significantly lower in hGL cells from bPOI patients than in those form controls (Fig. 6H).

YBX1 maintains the stability of target transcripts in an m^{5}C-dependent manner

We performed an m^{5}C-MeRIP-qPCR assay to determine the changes in m^{5}C methylation levels of *CCND1*, *CCNE1*, and *RCC1* transcripts. We observed a significant enrichment of these transcripts in the m^{5}C IP groups compared with IgG IP groups (Fig. 7A–C). Moreover, YBX1 knockdown resulted in a decrease in the enrichment of these mRNAs bound with the m^{5}C-specific antibody (Fig. 7A–C). In addition, we demonstrated that the mRNA half-lives of *CCND1*, *CCNE1* and *RCC1* were significantly shorter in YBX1-KD KGN cells than in control cells (Fig. 7D–F).

Interestingly, our m^{5}C-MeRIP-seq results revealed that the m^{5}C modification sites in a subset of transcripts were located in the 5'-untranslated region (5'UTR). Given that m^{5}C modifications at the 5'UTR may also influence transcript stability [37], we further investigated whether YBX1

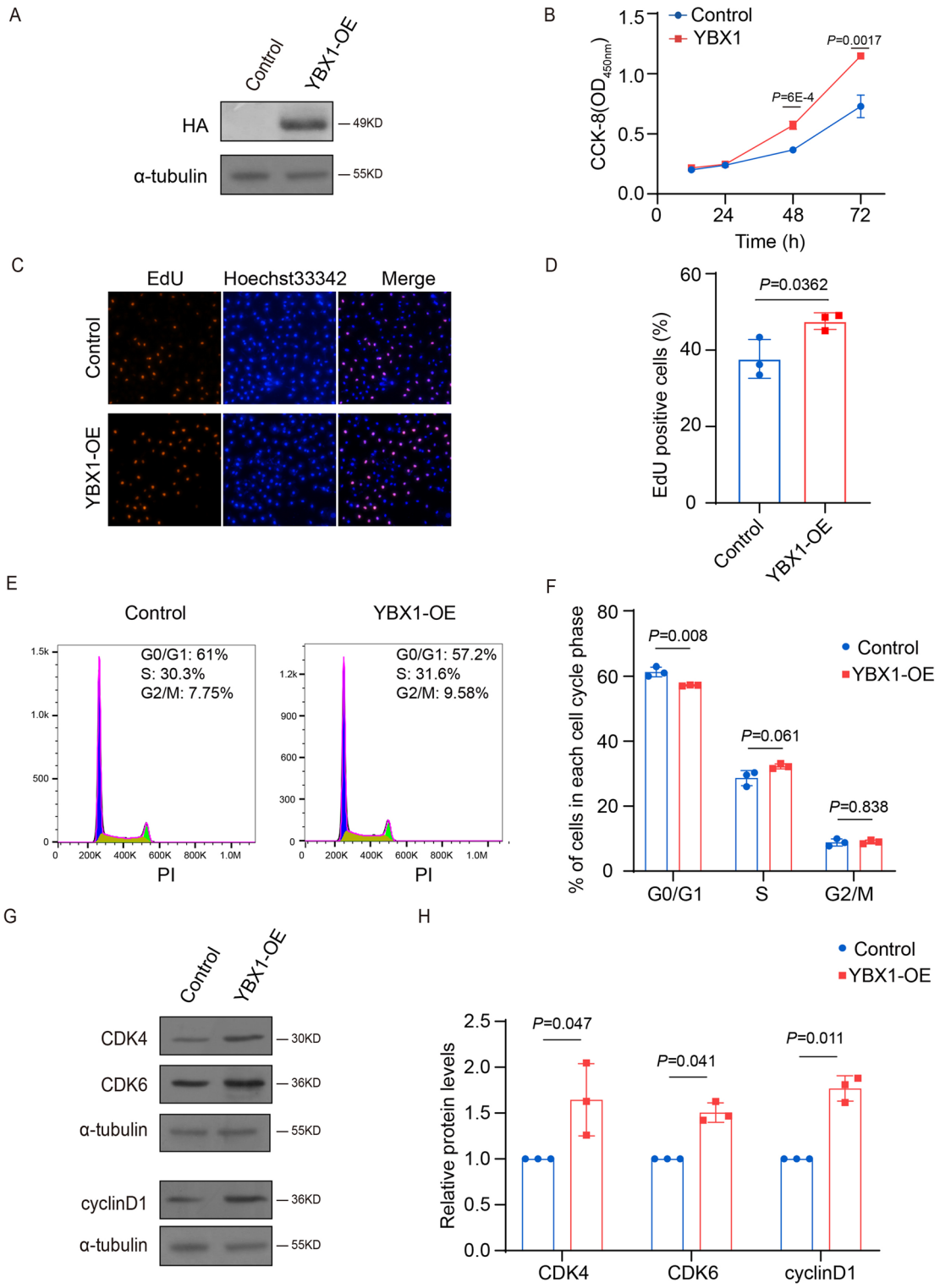

Fig. 3 YBX1 overexpression promotes cell cycle progression in human granulosa cells. **A** Level of YBX1-HA in KGN cells following transfection with the YBX1-HA plasmid was detected by western blot. **B** Effects of *YBX1* overexpression on KGN cells proliferation were measured using the CCK-8 assay. Data are presented as mean ± SD (n = 3). **C** The EdU staining revealed the proliferative ability of KGN cells after *YBX1* overexpression. Cells were detected using Hochest staining (blue), while the proliferating cells were identified through EdU staining (red). **D** The percentage of EdU-positive cells in the staining was determined. Data are presented as mean ± SD (n = 3). **E**, **F** The cell cycle distribution of KGN cells after *YBX1* overexpression was assessed using flow cytometry. Data are presented as mean ± SD (n = 3). *P* value, two-tailed Student's *t* test. n defines technical replicates. *OE* overexpression

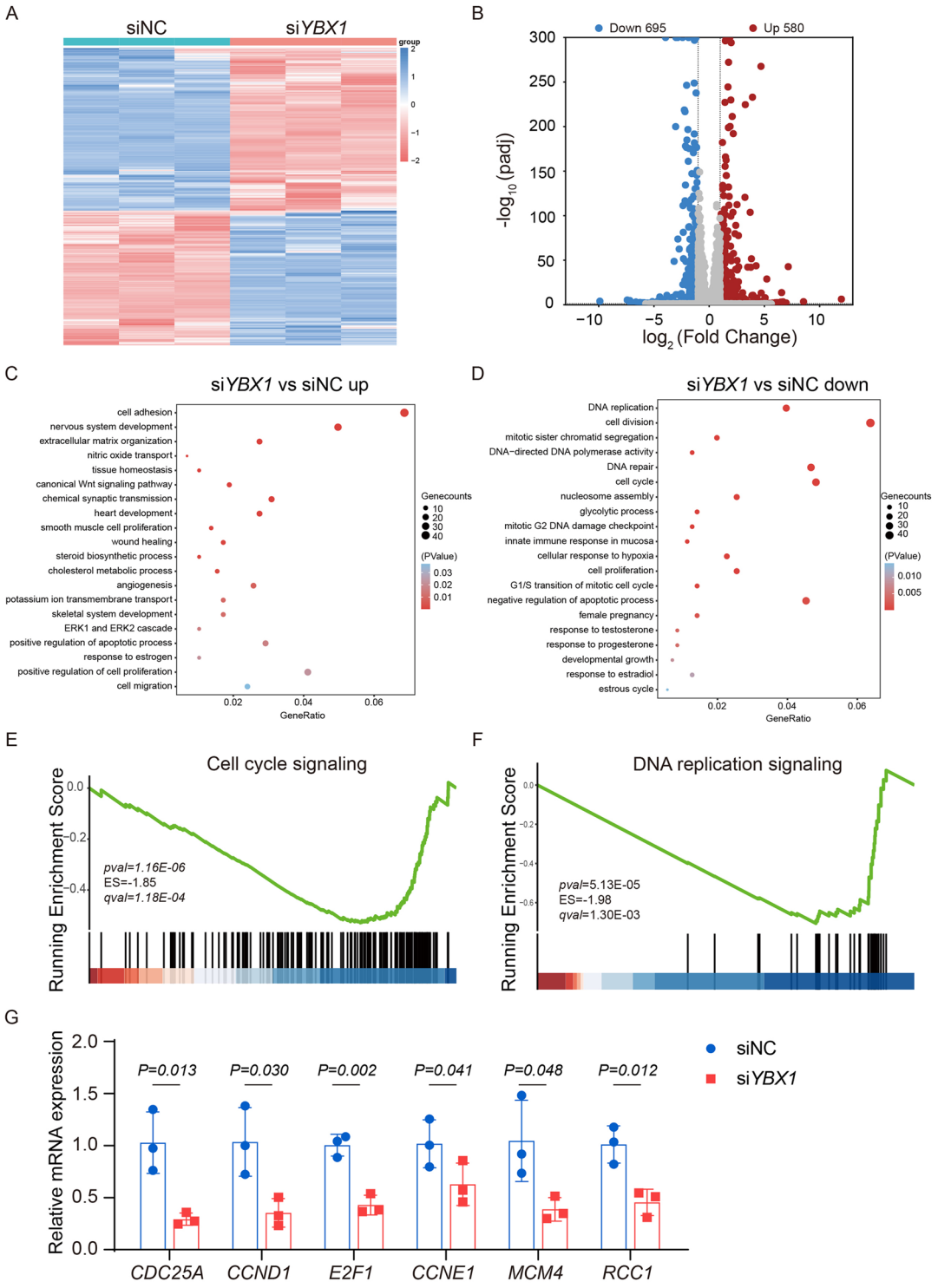

Fig. 4 Inhibition of YBX1 expression changes the transcriptome in human granulosa cells. **A** Heatmap generated from RNA-seq data depicted the representatively downregulated or upregulated transcripts in controls compared to *YBX1* knockdown KGN cells. **B** Volcano plot depicted RNA-seq data in *YBX1* knockdown KGN cells compared to non-targeting siRNA controls, with significantly downregulated transcripts (fold change <0.5, padj <0.05) in blue and significantly upregulated transcripts (fold change >2, padj <0.05) in red. And the transcripts of no difference are in grey. **C**, **D** GO analysis revealed the upregulated and downregulated expressed genes between *YBX1* knockdown and control KGN cells. The representatively 20 terms are reported. **E**, **F** GSEA showed a correlation between YBX1 expression and representative biological processes including cell cycle and DNA replication. **G** The mRNA expression levels of representative downregulated transcripts were examined by qRT-PCR in *YBX1* knockdown KGN cells. Data are presented as mean ± SD (n = 3). *P* value, two-tailed Student's *t* test. n defines technical replicates. *NC* negative control

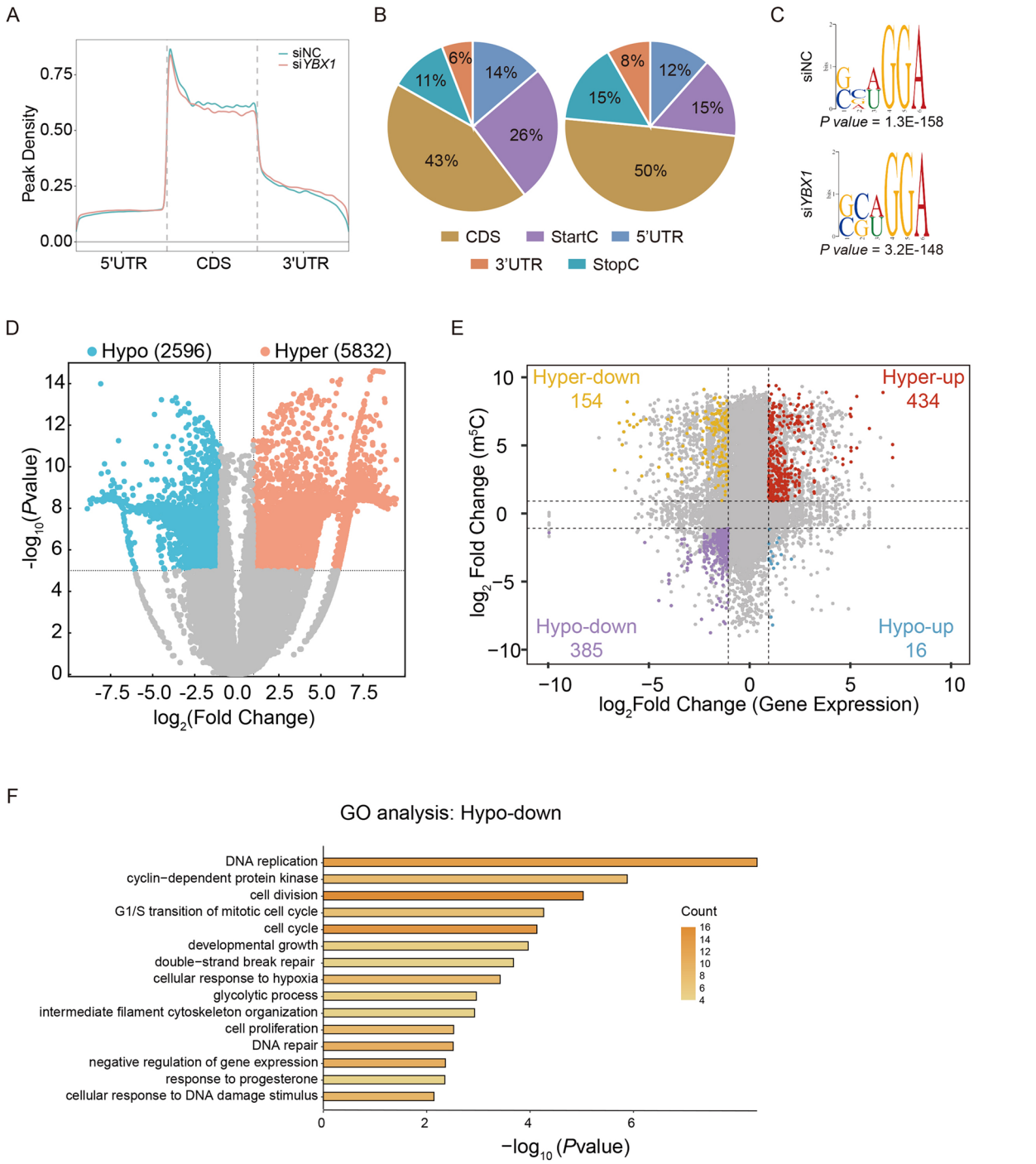

Fig. 5 YBX1 remodels the landscape of m^{5}C methylome in human granulosa cells. **A** The metagene profile illustrated the distribution of m^{5}C peaks along the entire length of transcripts, which were divided into three nonoverlapping segments: 5'-UTR, CDS, and 3'-UTR, with each segment rescaled accordingly. **B** The pie chart depicted the distribution of m^{5}C peaks in different transcript segments in control and *YBX1* knockdown KGN cells. **C** Top consensus m^{5}C motifs were detected by HOMER motif analysis in control and *YBX1* knockdown KGN cells with MeRIP-seq data. **D** Volcano plot illustrated MeRIP-seq data in *YBX1* knockdown KGN cells compared to non-targeting siRNA controls, highlighting significantly hypermethylated peaks in transcripts (fold change > 2, p value < 0.05) in light brown and significantly hypomethylated peaks in transcripts (fold change < 0.5, p value < 0.05) in bright blue. Transcripts showing no significant difference in methylation are represented in grey. **E** Four-quadrant diagram showed correlation between the gene expressions and the m^{5}C levels in control and *YBX1* knockdown KGN cells with MeRIP-seq data. **F** GO analysis of the hypo-m^{5}C methylation and downregulated expression (hypo-down) genes in control and *YBX1* knockdown KGN cells, as indicated in **D**. The representatively 15 terms are reported. Data are presented as mean ± SD (n = 3). *P* value, two-tailed Student's *t* test. n defines technical replicates. *NC* negative control

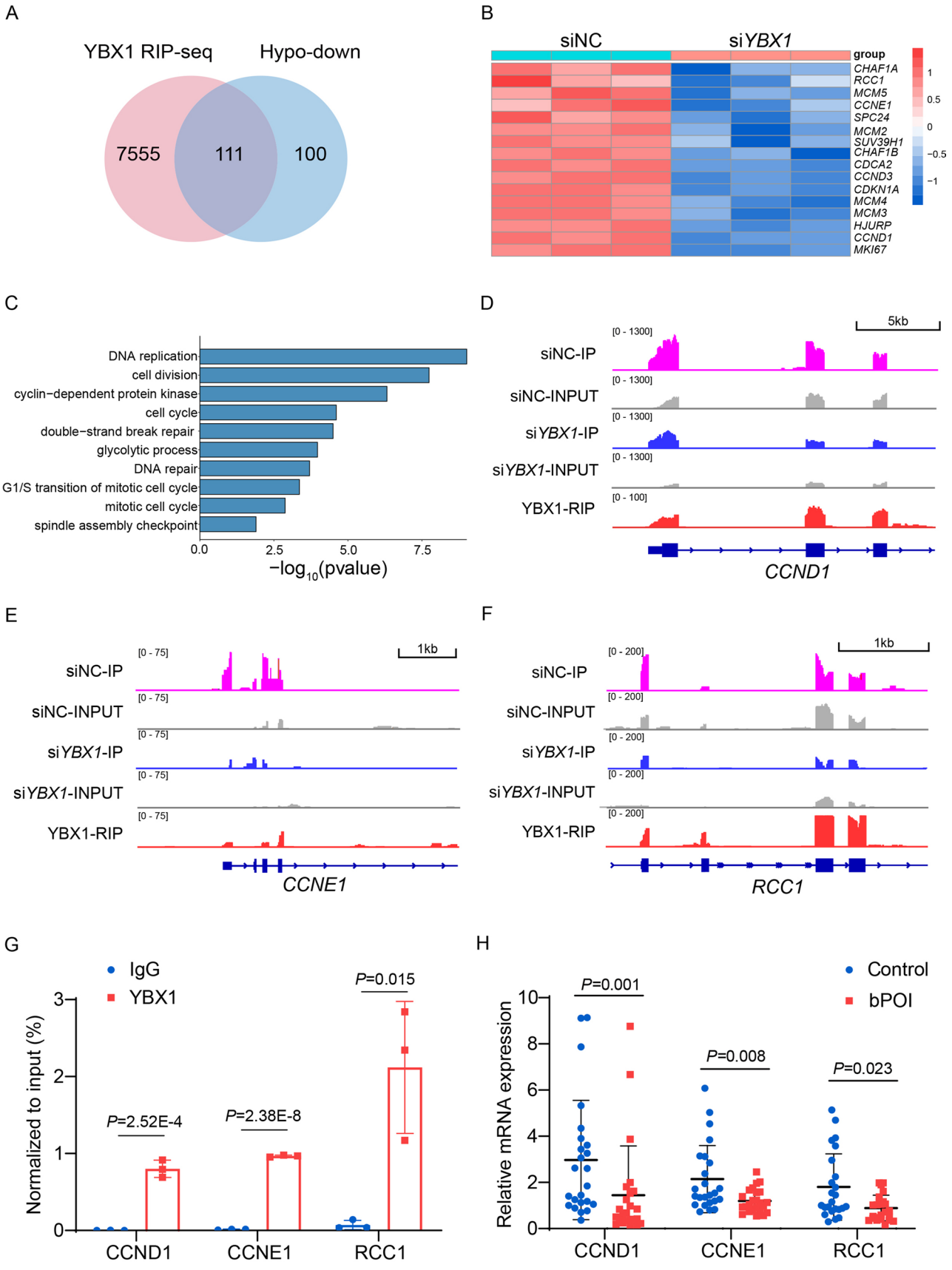
A
YBX1 RIP-seq
Hypo-down
7555
111
100
B
siNC
siYBX1
group
CHAF1A
RCC1
MCM5
CCNE1
SPC24
MCM2
SUV39H1
CHAF1B
CDCA2
CCND3
CDKN1A
MCM4
MCM3
HJURP
CCND1
MKI67
1
0.5
0
−0.5
−1
C
DNA replication
cell division
cyclin−dependent protein kinase
cell cycle
double−strand break repair
glycolytic process
DNA repair
G1/S transition of mitotic cell cycle
mitotic cell cycle
spindle assembly checkpoint
0.0
2.5
5.0
7.5
−log10(pvalue)
D
5kb
siNC-IP
siNC-INPUT
siYBX1-IP
siYBX1-INPUT
YBX1-RIP
[0 - 1300]
[0 - 100]
CCND1
E
1kb
siNC-IP
siNC-INPUT
siYBX1-IP
siYBX1-INPUT
YBX1-RIP
[0 - 75]
CCNE1
F
1kb
siNC-IP
siNC-INPUT
siYBX1-IP
siYBX1-INPUT
YBX1-RIP
[0 - 200]
RCC1
G
IgG
YBX1
Normalized to input (%)
P=2.52E-4
P=2.38E-8
P=0.015
CCND1
CCNE1
RCC1
H
Control
bPOI
Relative mRNA expression
P=0.001
P=0.008
P=0.023
CCND1
CCNE1
RCC1

◂**Fig. 6** Identification of YBX1 binding targets by sequencing data integration analysis. **A** Venn diagram showed the overlay of YBX1-binding target mRNAs with transcripts displaying hypo-m^{5}C methylation and downregulated expression following *YBX1* knockdown in KGN cells. **B** Heatmap generated from RNA-seq data depicted the representatively overlay of transcripts in controls compared to YBX1 knockdown KGN cells. **C** GO analysis was performed on the genes that exhibit overlap between YBX1-binding target mRNAs and hypo-down genes. The representatively 10 terms are reported. **D–F** Integrative-genomics-viewer tracks displayed the distributions of m^{5}C modifications, the read coverage and YBX1-binding clusters among CCND1, CCNE1, and RCC1. The m^{5}C enrichment in siNC and si*YBX1* IP samples, as well as the YBX1-binding clusters, were highlighted in pink, blue and red, respectively. **G** RIP-qPCR analysis showed the interactions between YBX1 and the indicated RNAs in KGN cells. IgG was used as an internal control. The bar is mean ± SD resulting from three independent experiments. Data are presented as mean ± SD (n = 3). n defines technical replicates. **H** The mRNA expression levels of *CCND1*, *CCNE1* and *RCC1* were determined by qRT-PCR in GCs from an independent cohort of controls (n = 24) and bPOI (n = 24). Data are presented as mean ± SD. n defines replicate samples. *P* value, two-tailed Student's *t* test. *NC* negative control

stabilized the transcripts by recognizing m^{5}C modification sites at the 5'UTR. Here, *CCND*1 was selected as an example for further study. Two key m^{5}C modification sites in *CCND1* were identified by our m^{5}C-MeRIP-seq (Fig. 7G). We then constructed wild-type (WT) and two point-mutated of *CCND1* 5'UTR luciferase reporter plasmids (Fig. 7G). The luciferase reporter assay revealed that the relative luciferase activity was significantly greater in the WT strain compared than in the control strain in the YBX1-overexpressing 293 T cells (Fig. 7H). In contrast, the relative luciferase activity did not differ between two mutants and the control in the YBX1-overexpressing 293 T cells (Fig. 7H). These results suggest that YBX1 also promotes RNA stability through its recognition of m^{5}C modification sites in the 5'UTR.

Discussion

The follicle, serving as the fundamental functional unit of the ovary, consists of the oocyte and the surrounding somatic cells. The GCs form a layer of somatic cells that connects directly to the oocyte. GCs provide nutrients, growth factors and steroids to promote oocyte maturation [38, 39]. GC Dysfunction results in follicle atresia and subsequent ovarian malfunction [40, 41]. A previous study revealed that a reduction in the level of the lncRNA HCP5 inhibits the nuclear entry of YBX1 in human GCs, suppressing the DNA damage repair ability of GCs by decreasing the expression of the DNA repair protein MSH5, which in turn results in the development of bPOI [21]. Furthermore, YBX1 can also interact with MALAT1, a long noncoding RNA, to promote its stability and facilitate ovarian restoration in both in vivo and in vitro POF models [22]. In this study, we observed a dramatic reduction in YBX1 expression in GCs from bPOI patients. Moreover, YBX1 silencing resulted in cell cycle arrest at the G1-S phase in KGN cells. Our study demonstrated that YBX1 per se can directly affect the proliferative ability of human GC.

A previous study demonstrated that YBX1 is a transcriptional activator that enhances gene expression during folliculogenesis [20]. FSH stimulation can quickly promote the phosphorylation of YBX-1 at Ser102, which is essential for FSH-mediated target gene expression [20]. In recent years, YBX1 has been identified as an m^{5}C reader [15, 42, 43]. The depletion of YBX1 impairs the development of zebrafish embryos and Drosophila ovarian germline stem cells by recognizing m^{5}C RNA [15, 42–44]. In the present study, we demonstrated another function of YBX1 in mediating the physiological activity of GCs, beyond its transcriptional regulation or lncRNA binding ability. YBX1 modulates GC proliferation by affecting the stability of cell cycle-associated genes in an m^{5}C-dependent manner (Fig. 8). One limitation is that the majority of data on the role of YBX1 in human GCs in the present study is derived from studies in KGN cells. As an immortalized human granulosa tumor cell line, KGN cells cannot fully accurately represent the nature of normal human granulosa cells. Furthermore, we explored the regulatory effects of YBX1 on human GC physiology only in vitro. Studying the essential role of YBX1 in ovarian function in vivo through animal models is necessary.

The quantity and quality of dormant oocytes in primordial follicles determine ovarian reserve. Both apoptosis and overactivation accelerate the exhaustion of the primordial follicle pool, resulting in POI. In recent decades, many POI-causative genes have been identified via the whole-exome sequencing (WES) in large pedigrees of families with POI [45]. However, genetic factors are present in only approximately 20–25% of patients, and the pathogenesis remains elusive in the majority of the POI population [46]. Epigenetics is considered an important candidate factor causing POI, which could lead directly to the occurrence of diseases without affecting the genomic DNA sequence. Thus, the role of epigenetic alternations in POI is of great interest. The function of RNA modifications, especially m^{6}A modifications, as a type of epigenetic modification in the female reproductive system has been adequately investigated in recent decades. Using germ cell-specific knockout mice, investigators have demonstrated the essential role of RNA-modifying proteins in the maintaining ovarian reserve [7]. Nevertheless, it is necessary to widen the network of POI candidate genes to include the key proteins that function within posttranscriptional regulatory networks. However, few genetic mutations within RNA modification protein coding genes have been found in POI patients, except for YTHDC2 mutations [47]. These findings seem inconsistent with the findings obtained

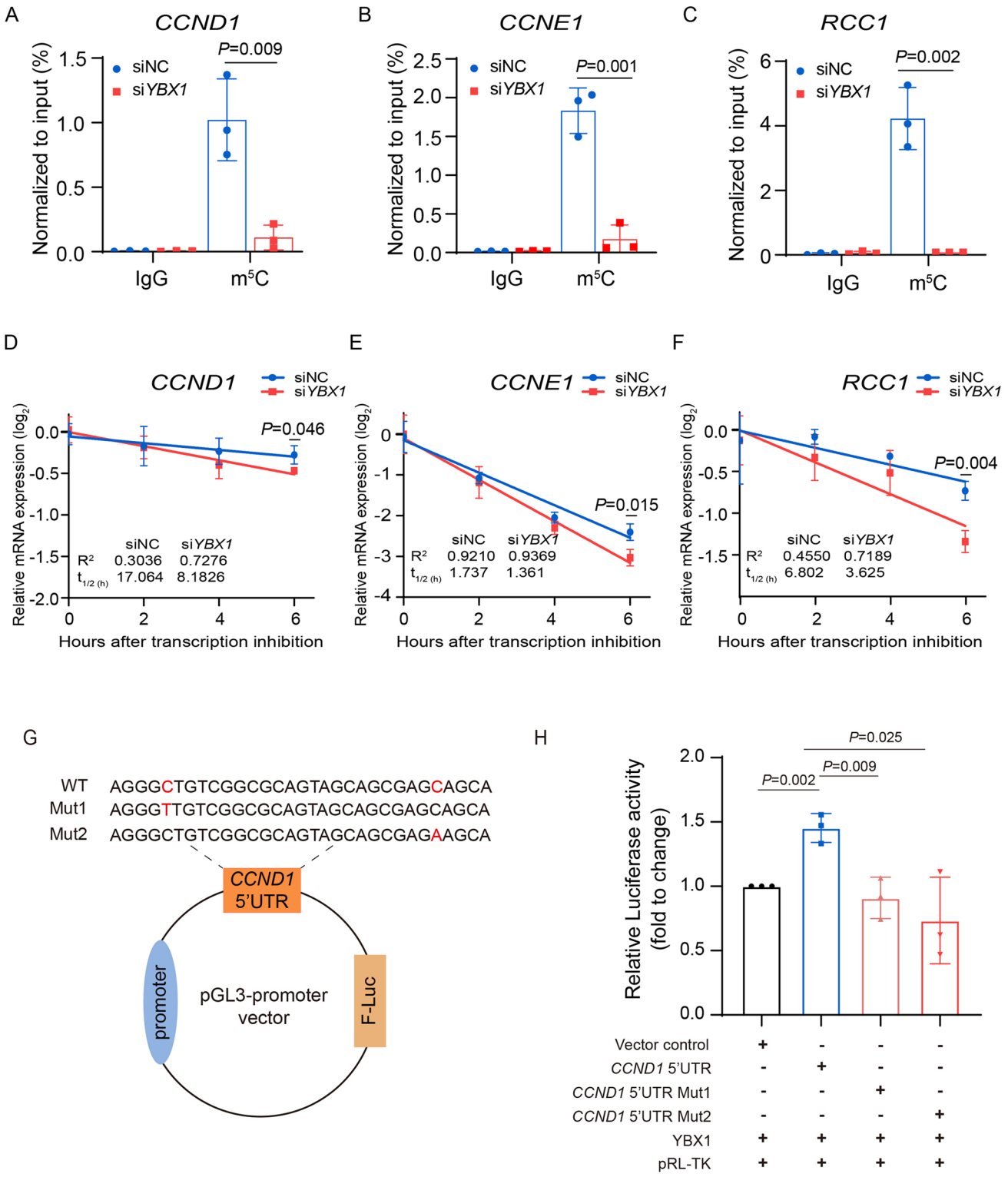

Fig. 7 YBX1 maintains the stability of target mRNA by recognizing m^5C modification. **A–C** RNA immunoprecipitation results validated the relative m^5C enrichments among the indicated genes in control and *YBX1* knockdown KGN cells. The data are validated by qPCR and presented as mean ± SD (n = 3). n defines technical replicates. **D–F** The decay curves showed the mRNA levels of *CCND1*, *CCNE1*, and *RCC1* after actinomycin D at the indicated time points in control and *YBX1* knockdown KGN cells. The data are validated by qPCR and presented as mean ± SD (n = 3). n defines technical replicates. **G** Schematic representation of the m^5C site and its mutants in the 5'UTR of *CCND1* mRNA. **H** Luciferase reporter assays showed that transfection of vector control, CCND1 5'UTR, or CCND1 5'UTR mutants (Mut1 and Mut2) with YBX1 and pRL-TK plasmids resulted in varying relative luciferase expression in HEK293 T cells. Data are presented as mean ± SD (n = 3). n defines technical replicates. *P* value, two-tailed Student's *t* test. *NC* negative control

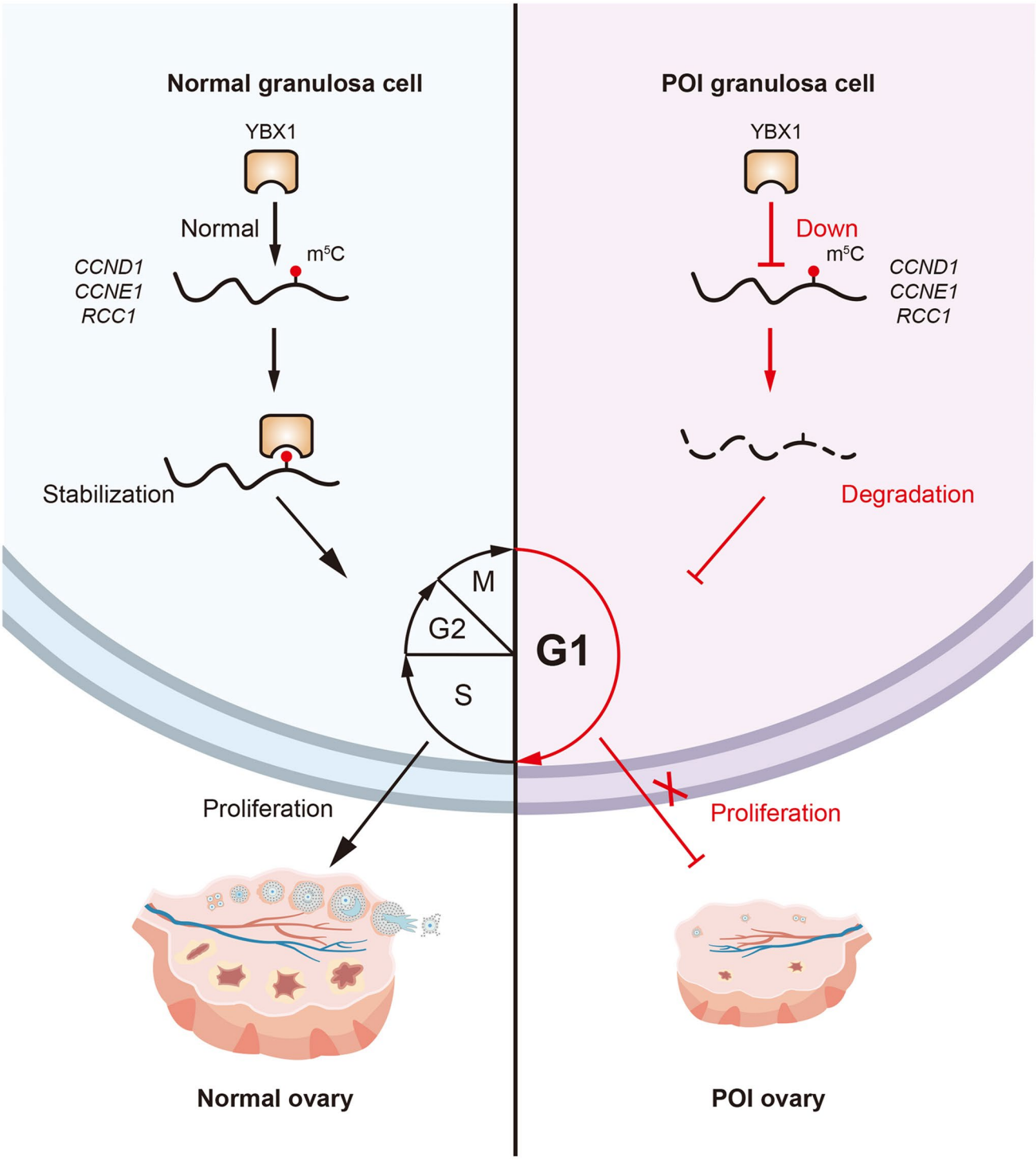

Fig. 8 Illustrations summarizing the molecular mechanism aberrant expression levels of YBX1 in GCs, resulting in the occurrence of POI. YBX1 participates in the regulation of hGL cell cycle progression by affecting the mRNA stabilization of *CCND1*, *CCNE1*, and *RCC1* in an m^5C-dependent manner. The aberrant downregulation of YBX1 alter the m^5C methylome, resulting in the destabilization of *CCND1*, *CCNE1*, and *RCC1*. The cell cycle will be arrested in G1 phase when these transcripts expression are decreased, which contributes to the occurrence of bPOI

from animal genetic models. In fact, most of transgenic mice with global knockout of key RNA modification components, including *YBX1*, exhibit embryonic lethality [15, 48–50]. Accordingly, in humans, mutations in genes with such broad functions can cause embryonic development failure. This has largely limited the utility of RNA modification proteins in genetic screening for POI. The identification of mutants associated with POI risk at the posttranscriptional level remains a challenge. Synergistic analysis of genotype–phenotype correlation is an efficient strategy for risk prediction, routine diagnosis and early intervention in POI.

In conclusion, we demonstrated that YBX1 expression was decreased in GCs from bPOI patients. Silencing *YBX1* expression in KGN cells disrupted their proliferative ability by preventing the G1 to S transition. Through an integrated analysis of the transcriptome and m^5C methylome profiles, we found that YBX1 knockdown destabilized the expression of the cell cycle-associated transcripts *CCND1*, *CCNE1* and *RCC1* in an m^5C-dependent manner. Our results highlight the role of YBX1-mediated m^5C modification in regulating RNA metabolism and human GC physiology, thereby providing new insight into the pathogenesis of POI.

Supplementary Information The online version contains supplementary material available at https://doi.org/10.1007/s00018-025-05709-6.

Acknowledgements We thank all the staff at the Department of Reproductive Endocrinology, Women's Hospital, School of Medicine, Zhejiang University, Key Laboratory of Reproductive Genetics (Ministry of Education) and Zhejiang Key Laboratory of Maternal and Infant Health, for their contributions to the study design and data collection.

Authors' Contributions L. B and YM. Z conceived the project and designed the experiments. QC. C, SS. W and M. Z performed and analyzed the bulk of the experiments. Y. X and Y. S helped to collect the primary hGL cells. QQ. C and ZK. L helped to perform the sequencing data analysis. QC. C and SS. W wrote the manuscript and L.B, and YM. Z revised it.

Funding This research was supported by the Key Research and Development Program of Zhejiang Province (2025 C02116 and 2021 C03100) and the Key laboratory of Women's Reproductive Health Research of Zhejiang Province (ZDFY2020-RG-0001) to YM. Z. This research was also supported the National Natural Science Foundation of China (82471666) to L. B.

Data availability statement The RNA-seq and m^5C-MeRIP-seq data in the present study have been deposited in SRA database under accession codes: PRJNA1046652. The sequencing data that support the findings of this study are available on request from the corresponding author. The data are not publicly available due to privacy or ethical restrictions. The datasets generated during and/or analyzed during the current study are available from the corresponding author on reasonable request.

Declarations

Conflict of interests The authors declare that they have no competing interests.

Ethical approval This study was approved by the Ethics Committee of Women's Hospital of Zhejiang University (File no. IRB-20230043-R).

Consent for publication All the authors of this article give consent for publication of the manuscript.

References

1. Mishra GD, Davies MC, Hillman S, Chung HF, Roy S, Maclaran K et al (2024) Optimising health after early menopause. Lancet 403(10430):958–968
2. Nelson LM (2009) Clinical practice. Primary ovarian insufficiency. N Engl J Med 360(6):606–614
3. Anreiter I, Mir Q, Simpson JT, Janga SC, Soller M (2021) New twists in detecting mRNA modification dynamics. Trends Biotechnol 39(1):72–89
4. Wiener D, Schwartz S (2021) The epitranscriptome beyond m(6) A. Nat Rev Genet 22(2):119–131
5. Roundtree IA, Evans ME, Pan T, He C (2017) Dynamic RNA modifications in gene expression regulation. Cell 169(7):1187–1200
6. Cui X, Li H, Huang X, Xue T, Wang S, Zhu X et al (2024) N(6)-Methyladenosine modification on the function of female reproductive development and related diseases. Immun Inflamm Dis 12(12):e70089
7. Huang E, Chen L (2023) RNA N(6)-methyladenosine modification in female reproductive biology and pathophysiology. Cell Commun Signal 21(1):53
8. Brzezicha B, Schmidt M, Makalowska I, Jarmolowski A, Pienkowska J, Szweykowska-Kulinska Z (2006) Identification of human tRNA:m5C methyltransferase catalysing intron-dependent m5C formation in the first position of the anticodon of the pre-tRNA Leu (CAA). Nucleic Acids Res 34(20):6034–6043
9. Sharma S, Yang J, Watzinger P, Kotter P, Entian KD (2013) Yeast Nop2 and Rcm1 methylate C2870 and C2278 of the 25S rRNA, respectively. Nucleic Acids Res 41(19):9062–9076
10. Yang X, Yang Y, Sun BF, Chen YS, Xu JW, Lai WY et al (2017) 5-methylcytosine promotes mRNA export—NSUN2 as the methyltransferase and ALYREF as an m(5)C reader. Cell Res 27(5):606–625
11. Ding C, Lu J, Li J, Hu X, Liu Z, Su H et al (2022) RNA-methyltransferase Nsun5 controls the maternal-to-zygotic transition by regulating maternal mRNA stability. Clin Transl Med 12(12):e1137

12. Liu D, Yamamoto T, Wang H, Minami N, Honda S, Ikeda S (2024) NSUN5 is essential for proper cell proliferation and differentiation of mouse preimplantation embryos. Reproduction 168(1):240079
13. Liu J, Huang T, Chen W, Ding C, Zhao T, Zhao X et al (2022) Developmental mRNA m(5)C landscape and regulatory innovations of massive m(5)C modification of maternal mRNAs in animals. Nat Commun 13(1):2484
14. Selmi T, Hussain S, Dietmann S, Heiss M, Borland K, Flad S et al (2021) Sequence- and structure-specific cytosine-5 mRNA methylation by NSUN6. Nucleic Acids Res 49(2):1006–1022
15. Yang Y, Wang L, Han X, Yang WL, Zhang M, Ma HL et al (2019) RNA 5-methylcytosine facilitates the maternal-to-zygotic transition by preventing maternal mRNA decay. Mol Cell 75(6):1188–1202
16. Sha C, Chen L, Lin L, Li T, Wei H, Yang M et al (2021) TRDMT1 participates in the DNA damage repair of granulosa cells in premature ovarian failure. Aging (Albany NY) 13(11):15193–15213
17. Gilbert WV, Bell TA, Schaening C (2016) Messenger RNA modifications: form, distribution, and function. Science 352(6292):1408–1412
18. Chen X, Li A, Sun BF, Yang Y, Han YN, Yuan X et al (2019) 5-methylcytosine promotes pathogenesis of bladder cancer through stabilizing mRNAs. Nat Cell Biol 21(8):978–990
19. Wen J, Zhu Q, Liu Y, Gou LT (2024) RNA modifications: emerging players in the regulation of reproduction and development. Acta Biochim Biophys Sin (Shanghai) 57(1):33–58
20. Donaubauer EM, Hunzicker-Dunn ME (2016) Extracellular Signal-regulated Kinase (ERK)-dependent Phosphorylation of Y-box-binding protein 1 (YB-1) enhances gene expression in granulosa cells in response to follicle-stimulating hormone (FSH). J Biol Chem 291(23):12145–12160
21. Wang X, Zhang X, Dang Y, Li D, Lu G, Chan WY et al (2020) Long noncoding RNA HCP5 participates in premature ovarian insufficiency by transcriptionally regulating MSH5 and DNA damage repair via YB1. Nucleic Acids Res 48(8):4480–4491
22. Zhang M, Xing J, Zhao S, Lu M, Liu Y, Lin L et al (2024) Exosomal YB-1 facilitates ovarian restoration by MALAT1/miR-211-5p/FOXO(3) axis. Cell Biol Toxicol 40(1):29
23. Nishi Y, Yanase T, Mu Y, Oba K, Ichino I, Saito M et al (2001) Establishment and characterization of a steroidogenic human granulosa-like tumor cell line, KGN, that expresses functional follicle-stimulating hormone receptor. Endocrinology 142(1):437–445
24. Gagliardi M, Matarazzo MRRIP (2016) RNA Immunoprecipitation Methods. Mol Biol 1480:73–86
25. Lv H, Zhang Z-M, Li S-H, Tan J-X, Chen W, Lin H (2020) Evaluation of different computational methods on 5-methylcytosine sites identification. Brief Bioinform 21(3):982–995
26. Li J, Huang Y, Yang X, Zhou Y, Zhou Y (2018) RNAm 5Cfinder: a web-server for predicting RNA 5-methylcytosine (m5C) sites based on random forest. Sci Rep 8(1):17299
27. Kechin A, Boyarskikh U, Kel A, Filipenko M (2017) cutPrimers: a new tool for accurate cutting of primers from reads of targeted next generation sequencing. J Comput Biol 24(11):1138–1143
28. Kim D, Langmead B, Salzberg SL (2015) HISAT: a fast spliced aligner with low memory requirements. Nat Methods 12(4):357–360
29. Anders S, Pyl PT, Huber W (2015) HTSeq–a Python framework to work with high-throughput sequencing data. Bioinformatics 31(2):166–169
30. Robinson MD, McCarthy DJ, Smyth GK (2010) edgeR: a Bioconductor package for differential expression analysis of digital gene expression data. Bioinformatics 26(1):139–140
31. Thorvaldsdóttir H, Robinson JT, Mesirov JP (2013) Integrative Genomics Viewer (IGV): high-performance genomics data visualization and exploration. Brief Bioinform 14(2):178–192
32. Zhang Y, Liu T, Meyer CA, Eeckhoute J, Johnson DS, Bernstein BE et al (2008) Model-based analysis of ChIP-Seq (MACS). Genome Biol 9(9):R137
33. Shen L, Shao N-Y, Liu X, Maze I, Feng J, Nestler EJ (2013) diffReps: detecting differential chromatin modification sites from ChIP-seq data with biological replicates. PLoS ONE 8(6):e65598
34. Bailey TL (2011) DREME: motif discovery in transcription factor ChIP-seq data. Bioinformatics 27(12):1653–1659
35. Dennis G, Sherman BT, Hosack DA, Yang J, Gao W, Lane HC et al (2003) DAVID: database for annotation, visualization, and integrated discovery. Genome Biol 4(5):P3
36. Feng M, Xie X, Han G, Zhang T, Li Y, Li Y et al (2021) YBX1 is required for maintaining myeloid leukemia cell survival by regulating BCL2 stability in an m6A-dependent manner. Blood 138(1):71–85
37. Chen Y, Jiang Z, Zhang C, Zhang L, Chen H, Xiao N et al (2024) 5-Methylcytosine transferase NSUN2 drives NRF2-mediated ferroptosis resistance in non-small cell lung cancer. J Biol Chem 300(4):106793
38. Park J-Y, Su Y-Q, Ariga M, Law E, Jin SLC, Conti M (2004) EGF-like growth factors as mediators of LH action in the ovulatory follicle. Science (New York, NY) 303(5658):682–684
39. Dumesic DA, Meldrum DR, Katz-Jaffe MG, Krisher RL, Schoolcraft WB (2015) Oocyte environment: follicular fluid and cumulus cells are critical for oocyte health. Fertil Steril 103(2):303–316
40. Dumaresq-Doiron K, Edjekouane L, Orimoto AM, Yoffou PH, Gushulak L, Triggs-Raine B et al (2012) Hyal-1 but not Hyal-3 deficiency has an impact on ovarian folliculogenesis and female fertility by altering the follistatin/activin/Smad3 pathway and the apoptotic process. J Cell Physiol 227(5):1911–1922
41. Yeung CK, Wang G, Yao Y, Liang J, Tenny Chung CY, Chuai M et al (2017) BRE modulates granulosa cell death to affect ovarian follicle development and atresia in the mouse. Cell Death Dis 8(3):e2697
42. Yu J, Zhang Y, Zhang J, Che P, Long G, Yang Z et al (2024) The m5C reader protein Ybx1 promotes axon growth by regulating local translation in axons. Development 151(23):202781
43. Zheng S, Hu C, Lin Q, Li T, Li G, Tian Q et al (2024) Extracellular vesicle-packaged PIAT from cancer-associated fibroblasts drives neural remodeling by mediating m5C modification in pancreatic cancer mouse models. Sci Transl Med 16(756):eadi0178
44. Zou F, Tu R, Duan B, Yang Z, Ping Z, Song X et al (2020) Drosophila YBX1 homolog YPS promotes ovarian germ line stem cell development by preferentially recognizing 5-methylcytosine RNAs. Proc Natl Acad Sci U S A 117(7):3603–3609
45. Jiao X, Ke H, Qin Y, Chen ZJ (2018) Molecular genetics of premature ovarian insufficiency. Trends Endocrinol Metab 29(11):795–807
46. Qin Y, Jiao X, Simpson JL, Chen ZJ (2015) Genetics of primary ovarian insufficiency: new developments and opportunities. Hum Reprod Update 21(6):787–808
47. McGlacken-Byrne SM, Del Valle I, Quesne Stabej PL, Bellutti L, Garcia-Alonso L, Ocaka LA et al (2022) Pathogenic variants in the human m6A reader YTHDC2 are associated with primary ovarian insufficiency. JCI Insight. 7(5):154671
48. Geula S, Moshitch-Moshkovitz S, Dominissini D, Mansour AA, Kol N, Salmon-Divon M et al (2015) Stem cells. m6A mRNA methylation facilitates resolution of naive pluripotency toward differentiation. Science 347(6225):1002–1006
49. Kasowitz SD, Ma J, Anderson SJ, Leu NA, Xu Y, Gregory BD et al (2018) Nuclear m6A reader YTHDC1 regulates alternative

polyadenylation and splicing during mouse oocyte development. PLoS Genet 14(5):e1007412
50. Mendel M, Chen KM, Homolka D, Gos P, Pandey RR, McCarthy AA et al (2018) Methylation of structured RNA by the m(6)A writer METTL16 is essential for mouse embryonic development. Mol Cell 71(6):986–1000 (**e11**)